Output Feedback Control for Lift Maximization of a Pitching Airfoil

Justin M. Lidard*, Debdipta Goswami†, David Snyder‡, Girguis Sedky§, Anya Jones¶, and Derek A. Paley‖
University of Maryland, College Park, MD, 20742, USA

This paper describes the implementation of the Goman-Khrabrov model for flow stagnation near an actuated airfoil with a feedback-controlled pitch rate for the purpose of maximizing the time-averaged unsteady lift. A nonlinear state-feedback control law is designed to stabilize unsteady pitching behavior. Linearization of the closed-loop system establishes the existence of a supercritical Hopf bifurcation, which gives rise to a stable limit cycle. Control gains that produce the greatest time-averaged lift achieve a 40% improvement from the maximum steady-pitch lift. An output feedback design assimilates noisy lift measurements to estimate the model states using a recursive Bayesian filter equipped with a discrete approximation of the Perron-Frobenius operator to accommodate the nonlinear dynamics. Empirical identification of physical system parameters is ongoing.

Nomenclature

A	=	Jacobian matrix of linearized system
C_L	=	lift coefficient
C_D	=	drag coefficient
f_0	=	steady-state flow stagnation function
$\mathbf{F}$	=	nonlinear model dynamics
K_s	=	stall intensity factor
k_1, k_2	=	control gains
P	=	Perron-Frobenius transfer operator
S^1	=	Circle group of dimension 1
T	=	period of limit cycle
x	=	flow stagnation point

*Undergraduate Research Assistant, Department of Aerospace Engineering. AIAA Student Member.
†PhD Candidate, Department of Electrical and Computer Engineering.
‡Former Undergraduate Research Assistant, Department of Aerospace Engineering. AIAA Student Member.
§PhD Candidate, Department of Aerospace Engineering. AIAA Student Member.
¶Associate Professor, Department of Aerospace Engineering. AIAA Associate Fellow.
‖Willis H. Young Jr. Professor of Aerospace Engineering Education, Department of Aerospace Engineering and Institute for Systems Research. AIAA Associate Fellow.

$\mathbf{z}$ = state vector

α = angle of attack

$\lambda_{1,2}$ = eigenvalues of linearized system

ρ = probability density function

σ = real part of eigenvalue

σ_M^2 = variance of lift coefficient measurements

τ = measurement time interval

τ_1, τ_2 = flow settling time constants

ϕ = phase shift on steady-state flow separation function

ω = imaginary part of eigenvalue

$\tilde{y}$ = measured lift coefficient

I. Introduction

Unsteady aerodynamics is currently driving research at the interface of fluid dynamics and control theory for low Reynolds number aircraft such as micro air vehicles (MAVs). The regulation and control of unsteady behavior is crucial for maintaining the stability of an MAV, which necessitates accurate modeling of their flight surfaces. When an airfoil is repeatedly pitched, unsteady flow features develop delaying the onset of stall. Moreover, a rapidly pitching airfoil will typically stall at a higher angle of attack than a statically pitched airfoil. While unsteady or dynamic stall has catalyzed the development of model characterization in fluid dynamics, an optimal control approach has not yet emerged. Periodic pitching induces hysteresis loops in the lift coefficient, whose amplitudes are proportional to pitching frequency and airfoil geometry. Earlier works [1–3] have utilized linear control laws to maximize the steady-state lift, whereas here we seek to maximize the time-averaged lift in this paper using a nonlinear control law.

Prior works have studied stabilization techniques for MAVs and airfoils encountering unsteady flow features. These works utilize linear control techniques to drive complex, often nonlinear, dynamical systems to local equilibrium points or a steady state. Williams et al. [1] presented a method for lift coefficient stability for a wing in an unsteady flow environment. They use flow control to realize a proportional-integral control loop. Sedky et al. [2] demonstrated transverse gust rejection for a finite wing in an experimental towing tank. Several works also present nonlinear control techniques to achieve lift actuation. Oduyela et al. [4] introduced articulated wings to create additional roll stability for MAVs during gust encounters. Bhatia et al. [5] performed an extensive study on the stabilization of a flapping-wing MAV in the presence of discrete gust encounters. They characterize the behavior of the nonlinear system in the neighborhood of equilibrium points using linearization. Greenblatt et al. [3] demonstrate a significant reduction in lift hysteresis using a sinusoidal flow actuator with a low-order model presented originally by Goman and Khrabrov [6],

which we adopt here.

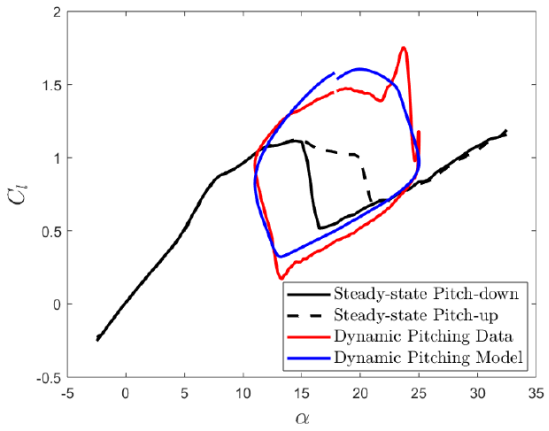

Figure 1 Dynamic stall characteristics of an airfoil, comparing model behavior with experimental results. An airfoil's pitch coefficient enters hysteresis loops near its stall angle as separation regions expand and collapse again [2].

.

The Goman-Khrabrov (GK) model is a low-order, nonlinear representation of the effect of unsteady flow features on lift based on two coupled first-order ordinary differential equations. Fig. 1 demonstrates the accuracy of the GK model in characterizing both static and dynamic pitching maneuvers for a wing, where dynamic pitching typically involves a periodic pitch rate. The lift hysteresis loops exhibited in Fig. 1 are typical of this type of pitching behavior [1, 3, 6]. Although current literature implements the GK model for purposes of active flow control and stabilization in unsteady flow, we examine the opposite approach: i.e., implementing a destabilizing behavior for the purpose of lift maximization. As [3] suggests, a time-varying control input, e.g., sinusoidal actuation, can reduce hysteresis effects and thereby decrease lift perturbations.

The technical approach of this paper is to design a feedback control of pitching rate in order to visit the high-lift regions of the GK-model state space using an unsteady pitch. By designing state and, eventually, output feedback controls, we eliminate the explicit time-dependence of the sinusoidal behavior, which allows us to formally characterize the oscillations as a stable limit cycle of the dynamics. We analyze the closed-loop system using tools from bifurcation analysis. Numerical results show that oscillating-pitch solutions boost the performance of the time-averaged lift by 40% over the best steady-pitch solution.

The contributions of this paper lie in the area of feedback control design for lift augmentation. The first novel contribution is the design of a nonlinear state-feedback control law to stabilize a limit cycle in the closed-loop Goman-Khrabrov model for flow separation. The optimal unsteady behavior compares favorably with the best-case steady-state behavior. Secondly, the state-feedback is extended to a dynamic output feedback design using a recursive Bayesian filter that assimilates noisy measurements of lift. The filter is implemented for the nonlinear dynamics using an

approximation of the Perron-Frobenius operator based on Constrained Ulam Dynamic Mode Decomposition (CU-DMD) [7]. The output feedback control performance is comparable to the state-feedback case when the measurement noise variance is sufficiently small.

The paper is organized as follows. Section II introduces the mathematical preliminaries of the GK model, Bayesian filtering, and the Perron-Frobenius transfer operator used in the output feedback control. Section III presents the state-feedback design to stabilize a limit cycle that maximizes lift. Section IV describes the results and limitations of a closed-loop GK system with output feedback, which emulates the conditions of laboratory testing. Section V summarizes the results and ongoing work.

II. Background on Model-based Dynamics and Estimation

A data-driven approach to studying unsteady flow features is effective at reducing the dimensionality of modeling representations [1–3, 8]. For example, the Goman-Khrabrov model provides a mechanism for characterizing flow separation on a wing based on static lift data. Section II.A introduces an analytic equation for the lift and drag coefficients and a modified state-space form of the Goman-Khrabrov model that permits a control input. Section II.B introduces the preliminaries of the recursive Bayesian filter and the Perron-Frobenius density transport operator so that the modified GK model may be implemented using output feedback.

A. The Goman-Khrabrov Model

This paper utilizes an adaptation of the Goman-Khrabrov (GK) model [6] for unsteady flow around an airfoil undergoing dynamic stall. The GK model is a two-state dynamical system consisting of an internal representation of the flow stagnation point $x \in [0, 1]$ and the angle of attack $\alpha \in S^1$ whose time evolution is defined by the following system of equations [6]:

$$\begin{aligned} \tau_1 \dot{x} + x &= f_0(\alpha - \tau_2 \dot{\alpha}) \\ \dot{\alpha} &= u, \end{aligned} \tag{1}$$

where the time constants τ_1 and τ_2 are the flow settling times and u is the control input. The stagnation function describes the state of separation as deduced from an airfoil's alignment to pre- and post-stall lift curves. The time rate of change for a dynamically pitching airfoil maps predictably as a function of angle of attack, but at higher or lower angles depending on the pitch rate.

The GK model is applicable to a wide class of airfoils. The stagnation function f_0 may be determined experimentally in order to capture airfoil geometry and flow constants, including the Reynolds number. While there is no known mathematical framework to derive f_0 from first principles, the boundedness of f_0 in the interval $[0, 1]$ can be used to produce an analytic approximation that captures its form and behavior. We elect to use an arctangent function with an

argument shift because of its simplicity when differentiated. The stagnation function used here is

$$f_0(\alpha - \tau_2\dot{\alpha}) = \frac{1}{2} - \frac{1}{\pi}\arctan\left(K_s(\alpha - \tau_2\dot{\alpha} - \phi)\right), \tag{2}$$

where K_s and ϕ are additional tuning parameters set according to stall characteristics. Fig. 2 compares this stagnation function to experimental data.

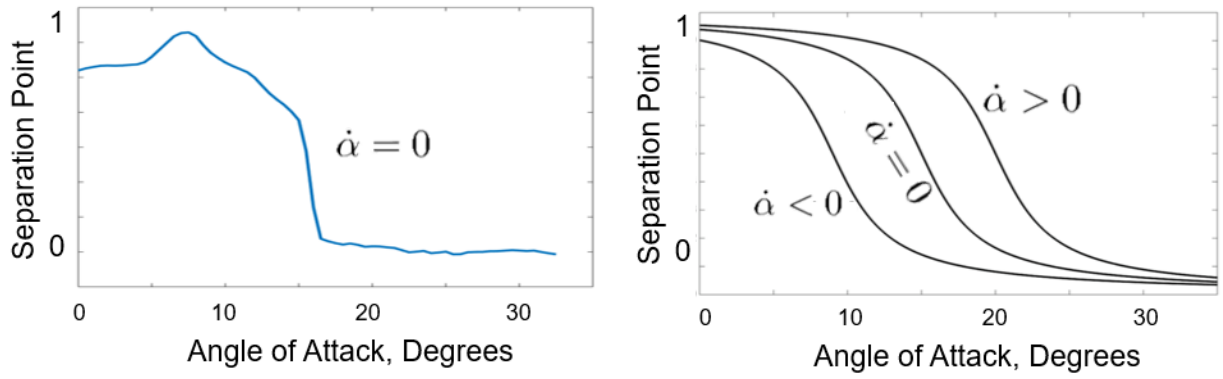

Figure 2 Comparison of stagnation function from (a) towing-tank data [2] and (b) analytic model using the arctangent.

A generalized model of the coefficient of lift C_L at high angles of attack as a function of the GK-model states x and α is [1, 3]

$$C_L = g_1(\alpha)x + g_2(\alpha)(1 - x), \tag{3}$$

where the functions $g_1(\alpha)$ and $g_2(\alpha)$ represent attached flow and fully separated flow, respectively. Note that Eq. (3) is linear in x. Goman and Khrabrov also present an analytic approximation for the coefficient of lift, based on assumptions that the separated flow is modeled by linear cavitation theory and Kirchhoff's zone of constant pressure [6]. In the original GK-model, the coefficient of lift is nonlinear in x and α, i.e., [6]

$$C_L = \frac{\pi}{2}(1 + \sqrt{x})^2 \sin\alpha. \tag{4}$$

While the general representation of C_L (3) is more readily applicable to airfoil data, we elect to model lift behavior here using (4) despite the nonlinearity, since it is analytic and can be differentiated directly.

Although thin airfoil theory fails to provide a closed-form analytic model for drag on an airfoil [9], the following model captures the dramatic increase in drag introduced by high angles of attack. Let C_{D0} represent the parasitic and form drag. The coefficient of drag is [9]

$$C_D = C_{D0} + \frac{C_L^2}{\pi e\,\mathrm{AR}}. \tag{5}$$

While the exact induced drag characteristics of the wing used in testing are not known precisely, the behavior of the drag coefficient is enough to characterize the drag produced at large angles of attack [9]. Small zero-lift drag is neglected to reflect the comparatively small effect of skin friction on the airfoil. A conservative span efficiency factor of $e = 0.7$ is used here to represent a non-elliptical planform.

The internal variable x can be derived from existing lift curve data for pre-stall and post-stall curves, where $x = 1$ represents fully attached flow and $x = 0$ denotes that the flow is fully separated. For example, a value of $x = 1$ returns a lift curve (4) identical to an airfoil's standard pre-stall trend. x is not a direct measurement of flow stagnation, as no information related to free-stream velocity, static pressure, or vorticity exists in this system. Rather, it can be thought of a representation of the flow attachment based on prior data-driven testing of the steady-state airfoil. Intermediate values between 0 and 1 reflect transient conditions. From (4), the nonlinear dependence of C_L on both α and x suggests that period oscillations in these parameters may produce lift that is higher, on average, than at constant α and x. This realization motivates a time-averaged, lift-maximizing control design using periodic pitching.

Let $\mathbf{z} = (z_1, z_2) \triangleq (x, \alpha)$ and $y \triangleq C_L$. In state-space form, the modified GK model is

$$\begin{aligned} \dot{z}_1 &= -\tfrac{1}{\tau_1} z_1 + \tfrac{1}{\tau_1}\left[\tfrac{1}{2} - \tfrac{1}{\pi}\arctan\left(K_s(\alpha - \tau_2\dot{\alpha} - \phi)\right)\right] \\ \dot{z}_2 &= u \\ y &= \tfrac{\pi}{2}(1 + \sqrt{z_1})^2 \sin z_2. \end{aligned} \tag{6}$$

In the sequel, we refer to the dynamics in (6) as $\dot{\mathbf{z}} = \mathbf{F}(\mathbf{z}, u)$. With regard to the input u, it is possible to use a sinusoidal controller in the form $u = A\sin(2\pi f t)$ to vary the pitch rate directly [3]. However, we seek below to derive a state feedback control of the form $u = u(\mathbf{z})$. Then we seek to implement this control using measurements of the output y to estimate z_1, assuming z_2 is known.

B. Recursive Bayesian Filtering

In order to implement an output feedback control for the system (6), we implement a recursive Bayesian filter to estimate $z_1 = x$ from measurements of $y = C_L$, assuming $z_2 = \alpha$ is known. This form of a filter is chosen because of the nonlinear dynamics and nonlinear output function in (6). A Bayesian framework allows the unknown state x to be inferred from the noisy measurements of the lift coefficient C_L together with the prior information accumulated in a probability density function [10]. In practice, measurements of the coefficient of lift of an airfoil can be obtained experimentally in a towing tank via a spring-gauge.

The first stage of a Bayesian filter, i.e., the prediction step, propagates the accumulated density according to the system dynamics. Because of the nonlinear dynamics, prediction is accomplished here by an offline approximation of the Perron-Frobenius (PF) transfer operator for this system [7]. We employ the discretized version of the PF operator that

works on a discretized prior. The prior density $\rho(z_1)$ is discretized using a grid on the state-space arranged in a vector resembling a probability mass function (PMF) $\mathbf{p}$. The discretized PF operator in form of a matrix P^τ operates over the PMF $\mathbf{p}$ to yield the updated prior $\mathbf{p}_\tau = \mathbf{p}P^\tau$, according to the dynamics. The time step of the motion update is small to keep the discretization error sufficiently small. The discretized approximation of the PF operator is computed using the Constrained Ulam Dynamic Mode Decomposition (CU-DMD) algorithm (see [7]), which is based on a combination of Ulam's Monte-Carlo method and Dynamic Mode Decomposition (DMD), to estimate the PF operator over a small time step.

The second stage of the Bayesian filter, i.e., the measurement step, involves the calculation of the posterior estimate using the conditional probability density known as the likelihood function. Let $\tilde{y}$ represent the noisy measurement of y. The Bayesian filter recursively calculates the posterior estimate $p(z_1|\tilde{y})$ according to Bayes' Theorem:

$$\rho(z_1|\tilde{y}) = \frac{\rho(\tilde{y}|z_1)\,\rho(z_1)}{\rho(\tilde{y})}. \tag{7}$$

For simplicity, assume that the lift-measurement noise is zero-mean Gaussian and the initial (prior) distribution is uniform. Also, the instantaneous angle-of-attack z_2 is known precisely, i.e., measured with zero variance.

III. Feedback Control Design for the Goman-Khrabrov Model

The Goman-Khrabrov model provides a reduced-order framework to design a state-feedback control that maximizes the time-averaged lift. This section describes a nonlinear state-feedback control law that drives the airfoil dynamics to a limit cycle whose parameters can be optimized using average lift as a metric. In contrast to an open-loop sinusoidal input, a state-feedback control is more robust in the presence of disturbances and model errors. Moreover, the closed-loop system is autonomous, which permits rigorous analysis in the phase plane.

To begin, consider the linear state-feedback controller, $u = -k_1 z_1 - k_2 z_2$, which drives the system to a static equilibrium point. However, using the GK lift coefficient (4), no steady pitch angle achieves the same lift performance as periodic pitching (see Fig. 3), which also avoids stall. Hence, we seek to stabilize a limit cycle by *destabilizing* the static equilibrium point. To accomplish this objective, consider the nonlinear state-feedback law

$$u = k_1 z_1 - k_2 z_2^3, \tag{8}$$

where k_1 and k_2 are positive control gains. Note that setting $k_1 < 0$ emulates stabilizing the linear control, using a cubic term for z_2 instead of a linear term. The closed-loop system (6) with the control (8) stabilizes a limit cycle for certain values of the gains k_1 and k_2. Fig. 3(left) depicts the nullclines for angle-of-attack, i.e., $\dot{z}_2 = 0$, for several values of the ratio k_2/k_1 superimposed on the heat map of the lift coefficient over the state space. Also shown is the open-loop

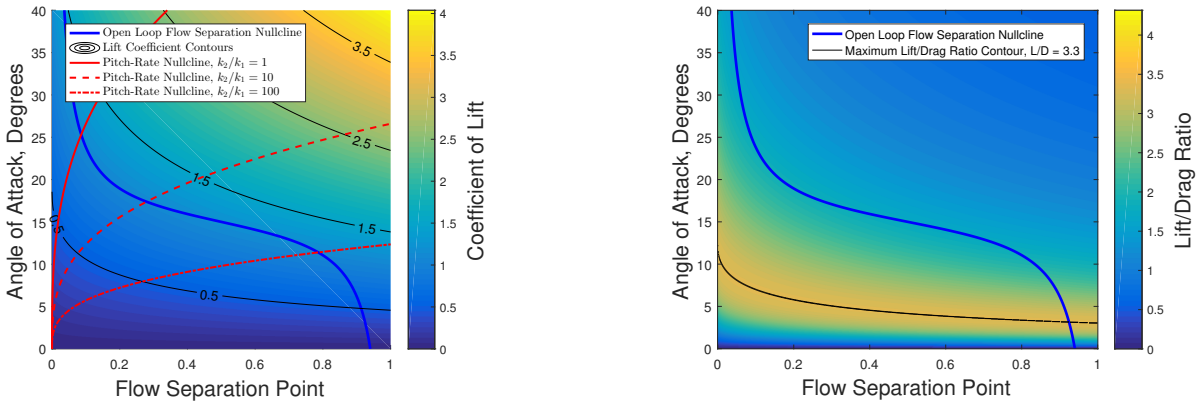

Figure 3 (Left) Lift coefficient in the phase plane. The open-loop flow separation nullcline (blue) represents the set of possible steady-state equilibrium points, which do not access the high lift regions (yellow). (Right) Color map depicting the lift-to-drag ratio as a function of the lift coefficient.

nullcline for the flow separation point, i.e., $\dot{z}_1|_{u=0} = 0$. Fig. 3(right) shows the same nullcline for the lift-to-drag ratio.

In order to establish the existence of a stable limit cycle in the closed-loop system, observe that the equilibrium points of the GK model satisfy $\dot{z}_1 = 0$ and $\dot{z}_2 = 0$, which implies

$$\frac{k_2}{k_1} z_2^3 = f_0(z_2). \tag{9}$$

Let z_2^* represent a solution to the equilibrium condition (9). The Jacobian of the closed-loop system evaluated at z_2^* is

$$A \triangleq \left.\frac{\partial \mathbf{F}}{\partial \mathbf{z}}\right|_{z_2=z_2^*} = \begin{bmatrix} \tau_1^{-1}\left(\dfrac{\tau_2^{-1}\pi^{-1}K_s k_1}{K_s(z_2^*-\phi)^2+1} - 1\right) & \dfrac{\tau_1^{-1}\tau_2^{-1}\pi^{-1}K_s(-3k_2(z_2^*)^2-\tau_2)}{K_s(z_2^*-\phi)^2+1} \\ k_1 & -3k_2(z_2^*)^2 \end{bmatrix}. \tag{10}$$

The eigenvalues of A are

$$\lambda_{1,2} = \frac{1}{2}\left(\operatorname{tr} A \pm \sqrt{\operatorname{tr}^2 A - 4\det A}\right). \tag{11}$$

If k_1 is allowed to vary while k_2 is held fixed, then the real and imaginary parts of the eigenvalue may be considered functions of the bifurcation parameter k_1, i.e.,

$$\lambda_{1,2} = \sigma(k_1) \pm \omega(k_1). \tag{12}$$

Fig. 4 illustrates how the eigenvalues of the closed-loop system cross the imaginary axis with nonzero velocity as the bifurcation parameter k_1 is increased. This behavior is consistent with a supercritical Hopf bifurcation [11], which gives

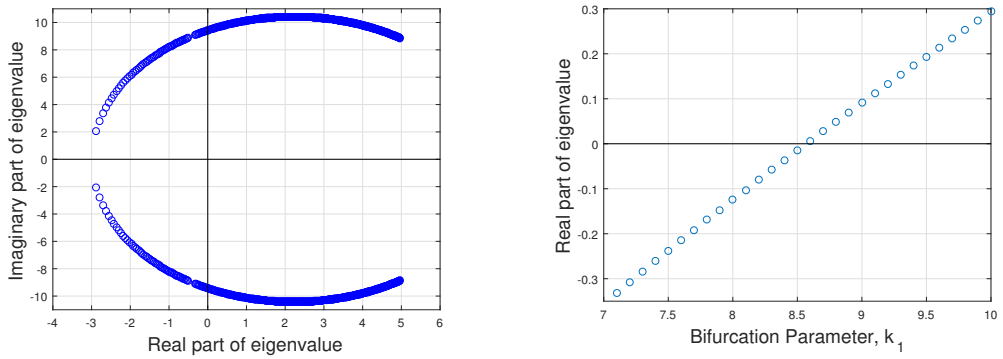

Figure 4 Poles of the linearized, closed-loop system as a function of the bifurcation parameter k_1. A Hopf bifurcation occurs when the real part of the eigenvalue crosses the imaginary axis away from zero.

rise to a stable limit cycle that corresponds to the desired oscillating trajectory. Fig. 5(left) shows the shape of the limit cycle in phase space. Note that it contains an unstable equilibrium point, and is thus attracting for interior points as well as the local neighborhood outside of it.

Figure 5(right) depicts the average-lift over all control gains k_1 and k_2 that stabilize a permissible limit cycle, i.e., a limit cycle that remains in the region of model validity. (Without loss of generality, assume an upper limit of 50° for the angle of attack; the analysis can be performed for any such limit.) To determine the optimal gains, time series simulation data of (z_1, z_2) were computed for a 100×100 grid of gain values.

The optimal gain for the model parameters is $(k_1, k_2) = (11.75, 22.8)$, which produces a time-averaged lift coefficient of $\bar{C}_L = 2.0$. The steady-state maximum possible lift coefficient is $\bar{C}_L = 1.43$ (see Fig. 3). Therefore, the nonlinear (unsteady) control performs approximately 40% better than linear (steady) control, using lift as a metric. However, the linear control performs better when using as metric the average ratio of lift to drag.

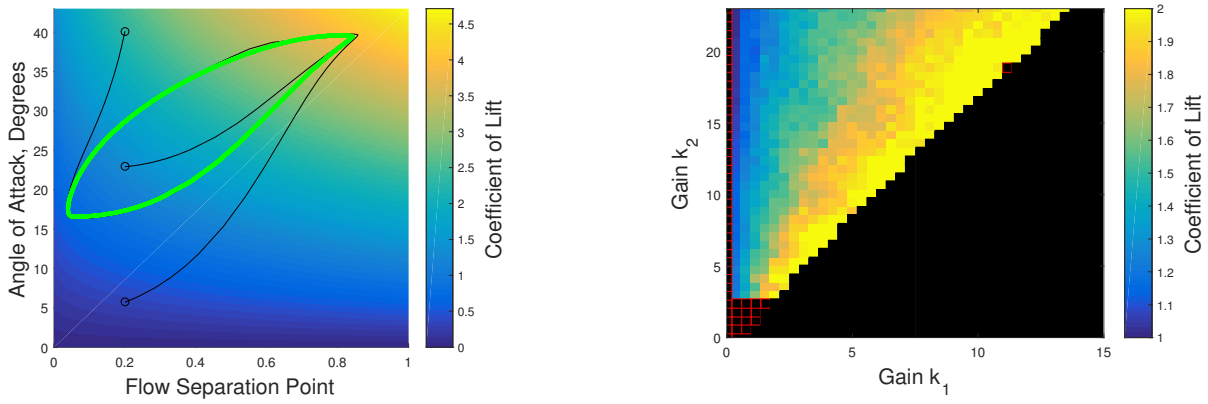

Figure 5 (Left) The stable limit cycle (green) in the closed-loop system attracts solutions that start inside or outside the limit cycle (black). (Right) Average lift performance of the closed-loop system for gain values that stabilize a limit cycle. Black squares indicate gains that fail to result in a permissible limit cycle. Red borders indicate gains that fail to produce a limit cycle at all.

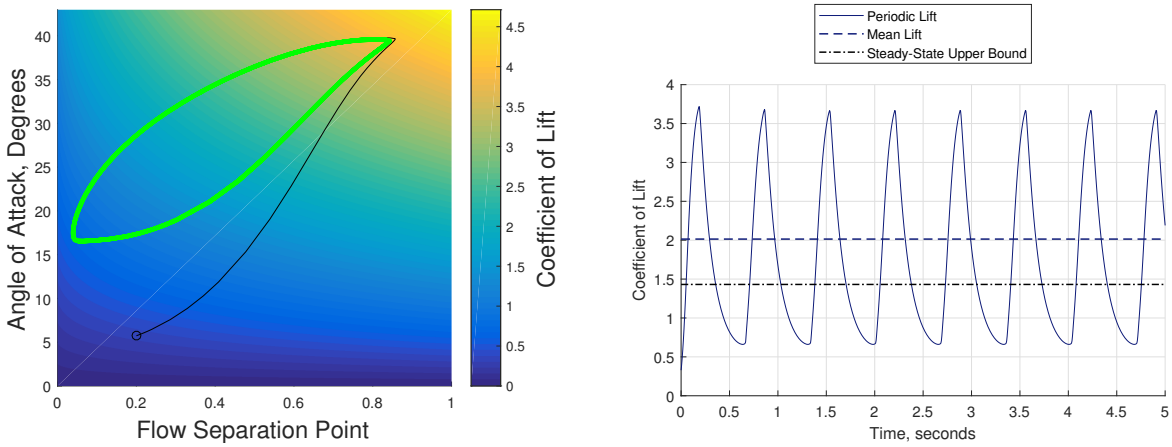

Figure 6 The lift-optimizing limit cycle (left) yields an average lift coefficient 40% higher than the steady-state upper bound (right).

IV. Output Feedback Control

The nonlinear control designed above is a state-feedback control that requires the precise values of the state variables to be available. However, state feedback control of this system is difficult or impossible to implement, because the flow-separation point z_1 is not measured directly. Here we design a filter to recursively estimate z_1 from noisy measurements of the lift coefficient $y = C_L$. Then we implement an output-feedback controller by replacing the state variable in the nonlinear controller with the estimated value $\hat{z}_1$.

Consider the state space equations (6). Let η be zero-mean uncorrelated Gaussian measurement noise with variance σ_M^2. The state and output equations have the general form

$$\begin{aligned} \dot{\mathbf{z}} &= \mathbf{F}(\mathbf{z}, u) \\ \tilde{y} &= y + \eta, \end{aligned} \tag{13}$$

where $\tilde{y}$ denotes the measured signal plus noise. These equations form the basis of a two-stage Bayesian filter with output feedback: the first equation describes the time evolution of the system states and the second allows them to be estimated from measurements. Assumed that the angle of attack $\alpha = z_2$ is measured precisely. With these assumptions, the likelihood function of the measurement $\tilde{y}$ given the flow separation point z_1 is

$$\rho(\tilde{y}|z_1) = \frac{1}{\sqrt{2\pi\sigma_M^2}} \exp\left(-\frac{(\tilde{y} - y(\mathbf{z}))^2}{2\sigma_M^2}\right). \tag{14}$$

To apply the Bayesian framework, we use motion and measurement updates periodically over time. In the motion update, the prior $\rho(z_1)$ is propagated using the dynamics (6) and the propagated prior is updated using Bayes' rule (7) when the

measurement $\tilde{y}$ arrives. The posterior is normalized to integrate to unity over the state space.

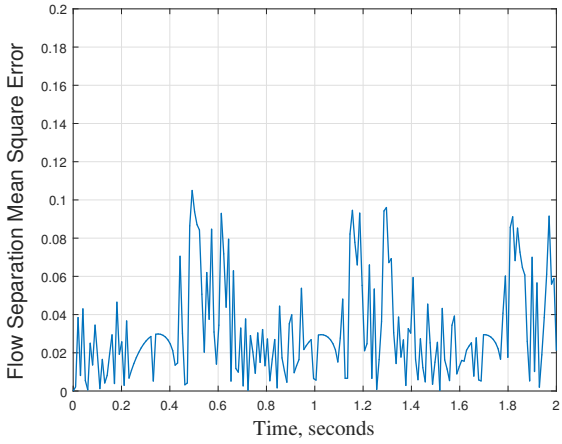

Figure 7 Mean-squared error of flow separation point using output feedback calculated over 100 Monte-Carlo simulations. Each simulation corresponds to 3 orbits of the limit cycle.

Because the equations of motion are nonlinear, we use a discretized version of the Perron-Frobenius (PF) operator [7, 12] with time step $\tau = 0.01$ and a size 30 grid on $z_1 = x$ for the motion update step. Constrained Ulam Dynamic Mode Decomposition (CU-DMD) [7] calculates the PF operator for 30 different control signals corresponding to the 30 grid points on the z_1 axis. For each $\tau = 0.01$, the discretized prior vector p is updated using the discretized PF matrix P^τ, and the mode of the prior $\hat{z}_1 = \underset{z_1}{\text{argmax}}\rho(z_1)$ is used as the estimate for the control design. After the Bayesian measurement update (7), the mode of the posterior $\hat{z}_1 = \underset{z_1}{\text{argmax}}\rho(z_1|\tilde{y})$ is used as the estimate as well. For each time step τ, the corresponding output-feedback control $u(\hat{z}_1, z_2)$ is used instead of the state-feedback control. Fig. 7 shows the mean-square error between the output- and the state-feedback controls for 100 Monte Carlo trials.

An important requirement of the output-feedback control is the preservation of the limit-cyclic behavior, which allows lift augmentation to continue indefinitely. Fig. 8 shows that the output-feedback control with discretized PF operator preserves the limit-cyclic structure of the state-feedback control, thereby preserving the high average lift. Adherence to the optimal limit cycle in each iteration is a function of the measurement noise covariance, as depicted in Fig. 8. Fig. 9 compares the lift coefficient time series obtained from the trajectories depicted in Fig. 8.

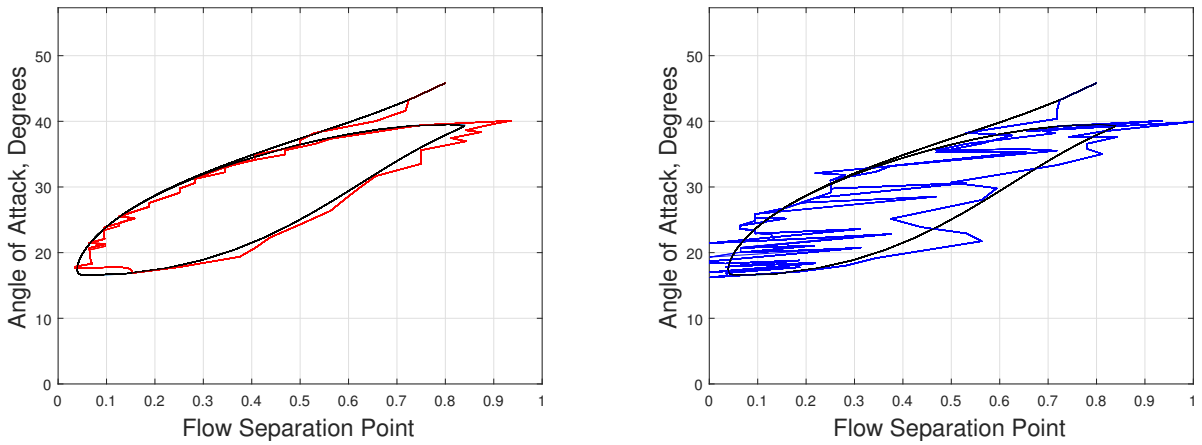

Figure 8 Limit cyclic behavior is preserved with output feedback, although adherence to the state feedback trajectory is a function of measurement noise σ_L: (left) $\sigma_M = 0.01$; (right) $\sigma_M = 0.1$

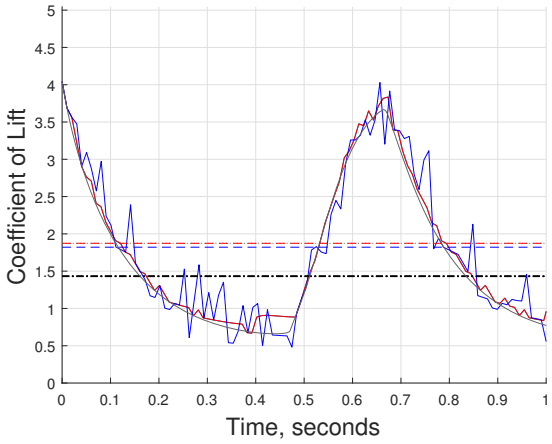

Figure 9 Coefficient of lift versus time for the trajectories in Fig. 8 (gray: state feedback, red: low noise, blue: high noise) and the optimal steady-state coefficient of lift (black). Time averages for each trajectory are shown with dashed lines of the same color.

V. Conclusion

This paper proposes state- and output-feedback controls for a pitching airfoil in an unsteady flow using the Goman-Khabrov model. Since the coefficient of lift undergoes hysteresis at or near stall, the proposed feedback control generates by design a stable limit cycle. The resulting periodic pitching trajectory yields a 40% increase in time-averaged lift, compared to the optimal steady pitch angle. However, a steady pitch angle maximizes the lift-to-drag ratio. In ongoing work, we seek to compare observer-based feedback strategies for online estimation of the model parameters. The chosen strategy will be used to implement an adaptive gain selection using a table of optimal gains for the model parameters.

Acknowledgments

This work was partially supported by AFOSR Grant No. FA9550-18-1-0137.

References

[1] Williams, D., Kerstens, W., Buntain, S., Quach, V., Prieffer, J., King, R., Tadmor, G., and Colonius, T., "Closed-Loop Control of a Wing in an Unsteady Flow," *48th AIAA Aerospace Sciences Meeting*, 2010. doi:10.2514/6.2010-358.

[2] Sedky, G., Jones, A., and Lagor, F., "Lift Modeling and Regulation for a Finite Wing during Transverse Gust Encounters," *AIAA Scitech 2019 Forum*, 2019, pp. 809–814. doi:10.2514/6.2019-1146.

[3] Greenblatt, D., Muller-Vahl, H., Srimanta, S., Williams, D., and Reissner, F., "Feed-forward Control for Goman-Khrabrov (G-K) Model on Pitching Airfoils with Flow Control," *8th AIAA Flow Control Conference*, 2016. doi:0.2514/6.2016-4240.

[4] Oduyela, A., and Slegers, N., "Gust Mitigation of Micro Air Vehicles Using Passive Articulated Wings," *The Scientific World Journal*, Vol. 2014, 2014, pp. 809–814. doi:http://dx.doi.org/10.1155/2014/598523.

[5] Bhatia, M., Patil, M., Woolsey, C., Stanford, B., and Beran, P., "Stabilization of Flapping-Wing Micro-Air Vehicles in Gust Environments," *Journal of Guidance, Control, and Dynamics*, Vol. 37, No. 2, 2014, pp. 592, 607. doi:https://doi.org/10.2514/1.59875.

[6] Goman, M., and Khrabrov, A., "State-Space Representation of Aerodynamic Characteristics of an Aircraft at High Angles of Attack," *AIAA Journal*, Vol. 31, No. 5, 1994, pp. 1109–1115. doi:10.2514/3.46618.

[7] Goswami, D., Thackray, E., and Paley, D. A., "Constrained Ulam Dynamic Mode Decomposition: Approximation of Perron-Frobenius Operator for Deterministic and Stochastic Systems," *IEEE Control Systems Letters*, Vol. 2, No. 4, 2018, pp. 809–814. doi:10.1109/LCSYS.2018.2849552.

[8] Gomez, D. F., Lagor, F. D., Kirk, P. B., Lind, A. H., Jones, A. R., and Paley, D. A., "Data-Driven Estimation of the Unsteady Flowfield Near an Actuated Airfoil with Embedded Pressure Sensors," *AIAA Scitech 2019 Forum*, 2019. doi:https://doi.org/10.2514/6.2019-0346.

[9] Anderson, J., *Fundamentals of Aerodynamics*, 5$^{\text{th}}$ ed., McGraw-Hill, New York, NY, 2007.

[10] Chen, Z. S., "Bayesian Filtering: From Kalman Filters to Particle Filters, and Beyond," *Statistics: A Journal of Theoretical and Applied Statistics*, Vol. 182, No. 1, 2003, pp. 1–69. doi:10.1080/02331880309257.

[11] Marsden, J. E., and McCracken, M., *The Hopf Bifurcation and its Applications*, 19$^{\text{th}}$ ed., Springer-Verlag, New York, NY, 1976.

[12] Klus, S., Koltai, P., and Schutte, K., "On the Numerical Approximation of the Perron–Frobenius and Koopman Operator," *Journal of Computational Dynamics*, Vol. 3, No. 1, 2016, pp. 51–79. doi:10.3934/jcd.2016003.